Supporting Information

Enhanced Thermoelectric Properties in Bulk Nanowire Heterostructure-based Nanocomposites through Minority Carrier Blocking

*Haoran Yang[1], Je-Hyeong Bahk[2], Tristan Day[3], Amr M. S. Mohammed[2, 4], G. Jeffrey Snyder[3], Ali Shakouri[2, 4] and Yue Wu[1, 5, *]*

** Corresponding Author*

** E-mail: yuewu@iastate.edu*

1. School of Chemical Engineering, Purdue University, West Lafayette, Indiana 47907, USA
2. Birck Nanotechnology Center, Purdue University, West Lafayette, Indiana 47907, USA
3. Materials Science, California Institute of Technology, Pasadena, California 91125, USA
4. School of Electrical and Computer Engineering, Purdue University, West Lafayette, Indiana 47907, USA
5. Department of Chemical and Biological Engineering, Iowa State University, Ames, Iowa, 50011 USA

This document includes the details of the experiments and the procedures for the theoretical modeling of the thermoelectric properties. Besides, the supplementary Figure S1 shows the lattice mismatch between Te (001) planes and PbTe (111) planes, and the supplementary Figure S2 shows the HRTEM images of the junctions between PbTe and Ag_2Te from four different heterostructures.

Experiments and Modeling Procedures

Synthesis of PbTe-Ag_2Te heterostructures. All chemicals are used as received without further purification. TeO_2 (≥99%), $Pb(CH_3CO_2)_2•3H_2O$ (≥99.99%) Polyvinylpyrrolidone (PVP for short, MW~40,000), KOH (90%), $N_2H_4•H_2O$ (78%~82%), are purchased from Sigma Aldrich, while $AgNO_3$ (≥99.9%), ethylene glycol (≥99%, EG for short) and ethanol (95%) are purchased from VWR. In a typical synthesis, 0.48 g TeO_2 (3 mmol), 0.6 g PVP, 2.24 g KOH, and 30 ml ethylene glycol are added to a 50 ml round bottom flask and heated to 140 °C. When the solution reaches 140 °C, 0.5 ml hydrazine hydrate is rapidly injected and nitrogen is applied to the reaction solution using a Schlenk line. Upon hydrazine hydrate addition, the reaction solution changes from transparent yellow to opaque black immediately. The reaction proceeds at 140 °C for 1 hour to allow the tellurium precursor to fully convert to tellurium nanowires. To grow PbTe on the two ends of each Te nanowires, 0.114 g (0.3 mmol) $Pb(CH_3CO_2)_2•3H_2O$ is dissolved in 2 ml ethylene glycol by heating to ~120 °C in a separate container. Meanwhile, the tellurium reaction solution is heated to 160 °C. The Pb precursor solution is injected into the tellurium reaction solution when the temperature of the reaction solution reaches 160 °C. The reaction proceeds for 1 hour at 160 °C after which the reaction solution is cooled to room temperature naturally. In the final step, the as-synthesized PbTe-Te heterostructures are washed 3 times with DI water and then re-dispersed in 35 ml ethylene glycol in a 100 ml beaker. In a separate container, 1.835 g (10.8 mol) $AgNO_3$ is dissolved in 10 ml ethylene glycol. The silver precursor solution is then slowly added to the tellurium nanowire solution and allowed to react for two hours under vagarious stirring. The products are then washed 3 times with DI water and then dispersed in ethanol or DI water for preparation of samples for XRD and TEM.

Hydrazine treatment and hot press. The hydrazine treatment and hot press processes are identical to our previous publication on Ag_2Te nanowires to allow the comparison of properties between the PbTe-Ag_2Te heterostructures and the Ag_2Te nanowires.[1] To remove the surface ligands, each batch of the Ag_2Te nanowires are dispersed in 40 ml ethanol and mixed with 4 ml N_2H_4•H_2O under vigorous stirring for a day. The nanowires are then collected with centrifugation and washed with DI water for three times. They are then dried at room temperature under vacuum and ground into loose powder in a nitrogen-filled glove box. For hot press, around 4 g nanowire powder is collected from 8 batches of synthesis, and is loaded into a 0.73 inch diameter stainless die in the glove box, compressed at a pressure of 165 MPa, heated to 150 °C and held at the same temperature for 20 minutes, and then cooled down to room temperature naturally.

Measurements of thermoelectric properties. The Seebeck coefficients of the hot-pressed samples are measured with a home-built Seebeck measurement system operated under vacuum, in which two heaters are used to control the overall temperature and to generate temperature difference between the hot and cold sides of the sample, and two type-K thermocouples are used to measure temperature and the voltage differences between the hot and cold sides of the sample. The electrical conductivity and Hall coefficients are measured on a custom-built Hall apparatus using van der Pauw geometry, and a 2 T magnetic field is used for Hall coefficient measurements.[2] Thermal diffusivity (a) measurements are completed using the laser flash method. Density (ρ) is determined by measuring sample dimensions and mass. Then thermal conductivity is calculated from the equation $\kappa = a * C_p * \rho$, where C_p stands for specific heat and the Dulong-Petit value ($3k_BT$ per atom) is used for C_p. The same treatment for C_p has been reported in several papers on Ag_2Te including ours.[1, 3-5]

Carrier transport modeling. Our transport model is based on the linearized Boltzmann transport equations (BTE) under the relaxation time approximation. The differential conductivity $\sigma_d(E)$ is defined as a function of energy by

$$\sigma_d(E) = e^2 \tau(E) v_x^2(E) \rho_{DOS}(E) \left(-\frac{\partial f_0(E)}{\partial E} \right), \tag{S1}$$

where e is the electron charge, τ is the relaxation time, ρ_{DOS} is the density of states, v_x is the carrier velocity in one direction, and f_0 is the Fermi-Dirac distribution. For the multiple-band transports in Ag_2Te, the transport properties are calculated in each of the bands with a relative position of the Fermi level from the band edge and the contributions from each band are then added together to find the total transport values in the bulk. The electrical conductivity σ, the Seebeck coefficient S, the Lorenz number L used in the Wiedemann-Franz relation, and the electronic thermal conductivity κ_e are given, respectively, as integral functions of the differential conductivity by

$$\sigma = \sum \int \sigma_d(E) dE, \tag{S2}$$

$$S = \sum \left(\frac{k_B}{q} \right) \int \left[\frac{(E - E_F)}{k_B T} \right] \frac{\sigma_d(E)}{\sigma} dE \ , \tag{S3}$$

$$L = \sum \frac{1}{\sigma} \left(\frac{k_B}{q} \right)^2 \int \left[\frac{E - E_F}{k_B T} \right]^2 \sigma_d(E) dE - S^2, \tag{S4}$$

$$\kappa_e = L \sigma T \ , \tag{S5}$$

where Σ is sum over the bands, q is $-e$ for conduction bands, and $+e$ for valence bands, T is the absolute temperature, and E_F is the relative position of the Fermi level to each of the band edge. (S5) is the Wiedemann-Franz relation.

For the transport modeling of Ag_2Te, both the conduction band and the valence band at the Γ valley in the Brillouin zone are taken into account as the bipolar transport is significant in this small band gap material. The band gap was assumed to be independent of temperature for the temperature range from room temperature to 400 K. The electron effective mass is temperature-dependent as $\sim T^{0.5}$ with $0.05m_0$ at 300 K.[3] Both the heavy and light hole effective masses are assumed to be constant, $0.32m_0$, $0.13m_0$, respectively in the temperature range.

According to our BTE calculations, the Lorenz number calculated by (S4) for the Ag_2Te samples is much lower than the conventional value (2.45×10^{-8} W Ω^{-1} K^{-2}). For the bare Ag_2Te sample, the Lorenz number steadily decreases from 1.48×10^{-8} to 1.17×10^{-8} W Ω^{-1} K^{-2} as temperature increases from 300 K to 390 K.

The relaxation time is determined by several major scattering mechanisms in Ag_2Te. Acoustic phonon deformation potential scattering, polar optical phonon scattering, and ionized impurity scattering are included in our calculations for bulk Ag_2Te, although it turns out that the acoustic phonon deformation potential scattering is a predominant scattering mechanism. In our nanostructured Ag_2Te, additional scattering mechanisms such as grain boundary and defect scatterings can be very strong and reduce the mobility quite significantly. We modeled this additional scattering using the short-range defect scattering and the ionized (long-range) impurity scattering mechanisms.

As discussed in the main text, we modeled the electron transport in the PbTe-Ag_2Te heterostructure nanocomposite by adding barrier heights in both the conduction and valence bands in the aforementioned Ag_2Te transport model. Since the atomic percentage of PbTe is less than 5 %, most of the transport is assumed to be occurring in the Ag_2Te matrix, and PbTe nano-inclusions simply act as heterostructure barriers. The Boltzmann transport equations with a

constant barrier height is discussed in details in our previous paper, Ref. 6. The barrier heights for electrons and holes are used as adjustable parameters to fit both the Seebeck coefficient and electrical conductivity of the samples over the entire temperature range. The barrier height is a measure relative to each of the band edge. We found that 110 meV and 45 meV barrier heights are best fitting the experimental data for electrons and holes, respectively as discussed in the main text of the paper.

Supplementary Figures

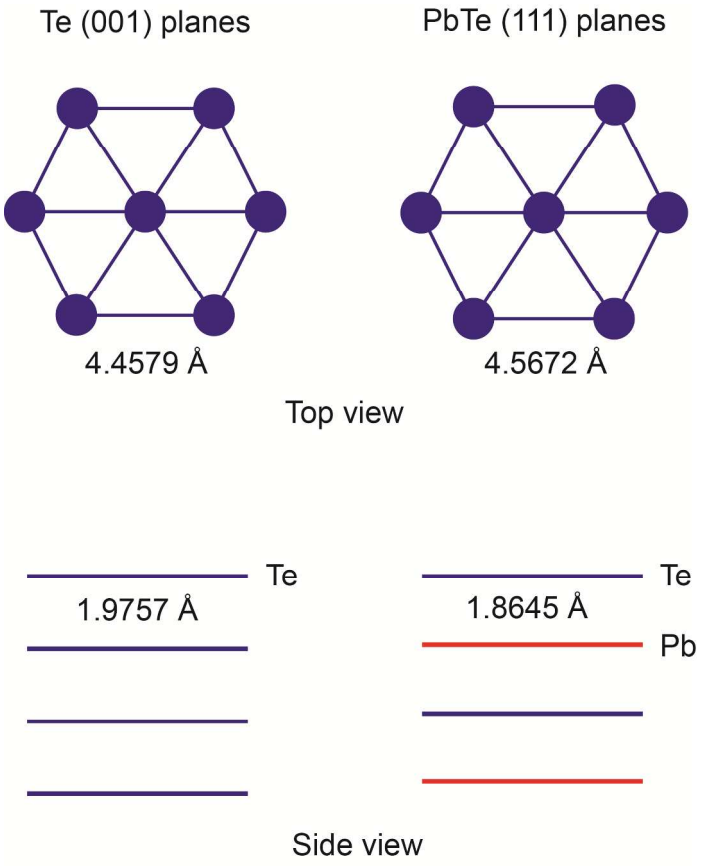

Figure S1. Schematic presentation of the lattice mismatch between Te (001) planes and PbTe (111) planes.

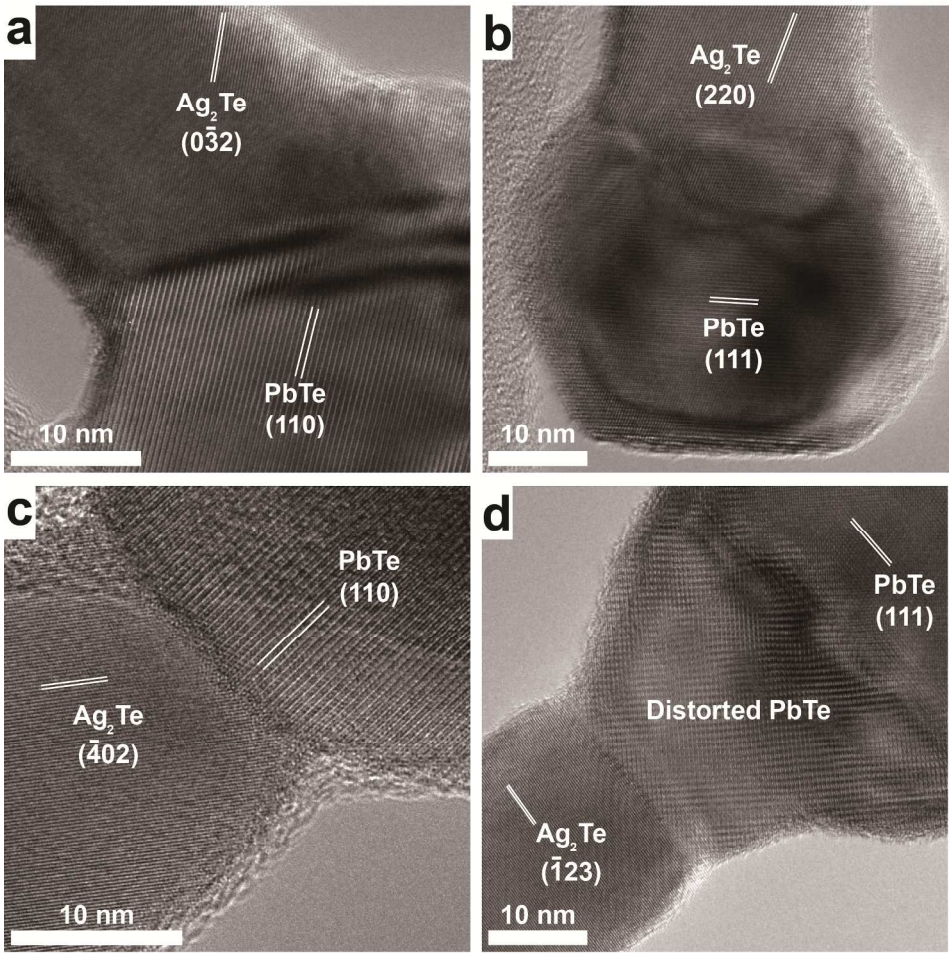

Figure S2. HRTEM images of the junctions between PbTe heads and Ag_2Te wires taken on several different PbTe-Ag_2Te heterostructures showing various features. (a) Ag_2Te partially incorporated into PbTe; (b) Ag_2Te forms a shell on PbTe; (c) Ag_2Te and PbTe forms a clear junction; and (d) distorted PbTe formed in between Ag_2Te and PbTe.

Supplementary Reference

(1) Yang, H.; Bahk, J.-H.; Day, T.; Mohammed, A. M. S.; Min, B.; Snyder, G. J.; Shakouri, A.; Wu, Y. *Nano Lett.* **2014**.

(2) Borup, K. A.; Toberer, E. S.; Zoltan, L. D.; Nakatsukasa, G.; Errico, M.; Fleurial, J.-P.; Iversen, B. B.; Snyder, G. J. *Review of Scientific Instruments* **2012,** 83, (12), 123902.

(3) Pei, Y.; Heinz, N. A.; Snyder, G. J. *Journal of Materials Chemistry* **2011,** 21, (45), 18256-18260.

(4) Cadavid, D.; Ibanez, M.; Shavel, A.; Dura, O. J.; Lopez de la Torre, M. A.; Cabot, A. *Journal of Materials Chemistry A* **2013,** 1, (15), 4864-4870.

(5) Jung, D.-y.; Kurosaki, K.; Ohishi, Y.; Muta, H.; Yamanaka, S. *MATERIALS TRANSACTIONS* **2012,** 53, (7), 1216-1219.

(6) Bahk, J.-H.; Bian, Z.; Shakouri, A. *Phys. Rev. B* **2013,** 87, (7), 075204.